

Article

Sulfur Nanoparticle-Decorated Nickel Cobalt Sulfide Hetero-Nanostructures with Enhanced Energy Storage for High-Performance Supercapacitors

Yedluri Anil Kumar ^{1,†} , Anuja A. Yadav ^{2,†}, Bandar Ali Al-Asbahi ³ , Seok-Won Kang ²  and Md Moniruzzaman ^{4,*}¹ Department of Physics, United Arab Emirates University, Al Ain 15551, United Arab Emirates² Department of Automotive Engineering, Yeungnam University, 280 Daehak-ro, Gyeongsan 38541, Gyeongbuk-do, Korea³ Department of Physics & Astronomy, College of Science, King Saud University, P.O. Box 2455, Riyadh 11451, Saudi Arabia⁴ Department of Chemical and Biological Engineering, Gachon University, 1342 Seongnam-daero, Seongnam-si 13120, Gyeonggi-do, Korea

* Correspondence: mani57chem@gachon.ac.kr; Tel.: +82-10-3261-0692

† These authors contributed equally to this work.

Abstract: Transition-metal sulfides exaggerate higher theoretical capacities and were considered a type of prospective nanomaterials for energy storage; their inherent weaker conductivities and lower electrochemical active sites limited the commercial applications of the electrodes. The sheet-like nickel cobalt sulfide nanoparticles with richer sulfur vacancies were fabricated by a two-step hydrothermal technique. The sheet-like nanoparticles self-combination by ultrathin nanoparticles brought active electrodes entirely contacted with the electrolytes, benefiting ion diffusion and charges/discharges. Nevertheless, defect engineers of sulfur vacancy at the atomic level raise the intrinsic conductivities and improve the active sites for energy storage functions. As a result, the gained sulfur-deficient NiCo₂S₄ nanosheets consist of good specific capacitances of 971 F g⁻¹ at 2 A g⁻¹ and an excellent cycle span, retaining 88.7% of the initial capacitance over 3500 cyclings. Moreover, the values of capacitance results exhibited that the fulfilling characteristic of the sample was a combination of the hydrothermal procedure and the surface capacitances behavior. This novel investigation proposes a new perspective to importantly improve the electrochemical performances of the electrode by the absolute engineering of defects and morphologies in the supercapacitor field.

Keywords: NiCo₂S₄; sulfur nanoparticle; electrode materials; supercapacitor; energy storage performance

Citation: Anil Kumar, Y.; Yadav, A.A.; Al-Asbahi, B.A.; Kang, S.-W.; Moniruzzaman, M. Sulfur Nanoparticle-Decorated Nickel Cobalt Sulfide Hetero-Nanostructures with Enhanced Energy Storage for High-Performance Supercapacitors. *Molecules* **2022**, *27*, 7458. <https://doi.org/10.3390/molecules27217458>

Academic Editor: Amor M. Abdelkader

Received: 22 September 2022

Accepted: 28 October 2022

Published: 2 November 2022

Publisher's Note: MDPI stays neutral with regard to jurisdictional claims in published maps and institutional affiliations.



Copyright: © 2022 by the authors. Licensee MDPI, Basel, Switzerland. This article is an open access article distributed under the terms and conditions of the Creative Commons Attribution (CC BY) license (<https://creativecommons.org/licenses/by/4.0/>).

1. Introduction

Worldwide, research is rising investigating safe, portable, renewable electrochemical electrical applications, and lightweight electrical gadgets, such as supercapacitors (SCs), which consider eco-friendly stabilities as well as higher energy/power densities [1–3]. In energy storage applications, supercapacitors (SCs) attained widespread consciousness on account of their extraordinary benefits in terms of rapid charging/discharging procedures, high reliability, excellent power densities, cheaper price, and environmental natures [4–7]. Meanwhile, the weaker energy densities of SCs have constricted them from laboratory scales to practical-span productivity [8–10]. Thus, higher performance sample-electrodes are worth finding for enhancing the energy densities of SCs.

Among them, transition-metal sulfides were advised as an essential source for the SCs application, owing to their higher capacity results, cheaper prices, innate abundances, and eco-friendliness [11]. Comparable to binary metal sulfides, bimetallic sulfide types (e.g., CuCo₂S₄ [12], NiCo₂S₄ [13], FeCo₂S₄ [14], MnCo₂S₄ [15]) normally manifest good added electrochemical behaviors for the given two causes: (i) the synergetic reaction of bimetallic sulfide types would consider a richer redox reaction; and (ii) bimetallic sulfide

types normally exhibit higher conductivities [16–18]. Nevertheless, the insufficient energy storage active sites and weaker ion diffusion kinetics were reasoned by the limit of ion diffusion connections, which led to poorer rate capabilities and specific capacities [19]. Recent research has been maintained to enhance the electrochemical performances of the samples' electrodes by morphology optimization and defect formations [20–22]. For instance, Wan et al. constructed NiCo_2S_4 porous nanotubes using sacrifices precursors to reason redox reactions at intrinsic activate sites, allow for faster ion transportations in the aqueous electrolyte, and represent a higher specific capacity of 933 F g^{-1} at 1 A g^{-1} [23]; Chen et al. fabricated caterpillar-type NiCoS crystals, exhibiting the higher specific capacitance of 1777 F g^{-1} at 1 A g^{-1} and retaining a 90.9% capacity of the starting cycles over 3000 cycles at 10 A g^{-1} [24]; Zhou et al. synthesized oxygen-deficient (V_o - ZnO/CoO) nanowires [25], in which the oxygen defect improves the redox processes, allowing for faster electron transportation rates; and Huang et al. fabricated $\text{NiS}@C$ with a sulfur vacancy ($\text{H-NiS}_{1-x}/C-50$), where the sulfur vacancy formations provide lattice distortion reactions, exhibiting improved conductivities and good electrochemical activities (1728 F g^{-1} , 1 A g^{-1}) [26]. Evidentially, the combination of sulfur-deficient NiCo_2S_4 with a conductive matrix-type nickel foam can enhance the cycling performances and rate capabilities of materials. Meanwhile, it has been noted that bimetallic nickel cobalt sulfide consists of numerous redox sites and abundant valence states [27]; therefore, it might be a favoring electrode applicant for SCs, in which its less efficient ion/electron transportations hinder the electrochemical activity. To the best of our understanding, the performances of a sulfur-deficient NiCo_2S_4 were not adequate, and it was the main endeavor to further boost the electrochemical activities of SCs. Compared to the recently reported composited bimetallic sulfides, it could be anticipated that the sulfur-deficient NiCo_2S_4 composite might provide stronger cooperative effects and assist volume alterations, promising to enhance the electrochemical performances for SCs applications.

Based on the above findings, we integrate deficient engineering with rational nanomorphology construction to grow sheet-like nickel cobalt sulfide nanoparticles, self-assembling by ultrathin nanoparticles with richer sulfur vacancies through hydrothermal treatment. The fabricated electrode consists of higher conductivities and numerous abundant activation sites, providing good specific capacitances of 971 F g^{-1} at 2 A g^{-1} and the 88.7% retained rate of the prior capacitances over 3500 long cycles. Moreover, the sulfur-deficient NiCo_2S_4 nanosheets electrode exhibits lower resistances, revealing the extraordinary current conductivity of the sample material. In the investigation, the interconnected nanoparticle-type sulfur-deficient NiCo_2S_4 nanosheets composite was illustrated to be perfect for SCs applications.

2. Materials and Methods

2.1. Reagents and Chemicals

Nickel nitrate hexahydrate ($\text{Ni}(\text{NO}_3)_2 \cdot 6\text{H}_2\text{O}$, 99.0%), cobalt nitrate hexahydrate ($\text{Co}(\text{NO}_3)_2 \cdot 6\text{H}_2\text{O}$, 98.6%), and sodium sulfide nonahydrate ($\text{Na}_2\text{S} \cdot 9\text{H}_2\text{O}$, 98.0%) were purchased by Sigma-Aldrich. All the chemicals were analytically graded and used without any further procedure. The nickel foam was pre-treated before being utilized.

2.2. Preparation of Sheet-like NiCo_2S_4 Nanoparticles with Richer Sulfur Vacancies on Ni Foam

In the preparation of sulfur-deficient sheet-like NiCo_2S_4 nanoparticles, 0.5 mmol $\text{Ni}(\text{NO}_3)_2 \cdot 6\text{H}_2\text{O}$, 0.9 mmol $\text{Co}(\text{NO}_3)_2 \cdot 6\text{H}_2\text{O}$, and 1.17 mmol $\text{Na}_2\text{S} \cdot 9\text{H}_2\text{O}$ were dissolved in 40 mL of DI water under continuous stirring to gain a pink product. Next, the Ni foam with product precursors was kept in a Teflon-lined stainless autoclave and optimized at $110 \text{ }^\circ\text{C}$ for 13 h. After reaching room temperature, the samples were rinsed with DI water and subjected to the drying process to gain the needed products. After being dried, the black precipitate product was annealed at $400 \text{ }^\circ\text{C}$ for 1 h in a furnace in a continual Ar atmosphere. The representative mass load of the sulfur-deficient NiCo_2S_4 composite was $\sim 2.6 \text{ mg cm}^{-2}$.

2.3. Characterizations and Instruments

The surface morphology and structures of the samples were observed using a scanning electron microscope (SEM, JSM-7800F equipping) and transmission electron microscopy (TEM, JEM-2100F, Busan, Korea). The crystal structures of the samples were determined using characteristic diffraction peaks measured by X-ray diffraction (XRD) analysis, which was performed using Bruker D8 Advance. X-ray photoelectron spectroscopy (ESCALAB 250Xi, Busan, Korea) was organized to investigate the chemical bonding details of the electrodes.

2.4. Electrochemical Performance Test

The evaluation of all the electrochemical calculations for the electrodes was organized in 3: an electrode setup employing the current precursor products as the working electrodes, Platinum (Pt) sheet as the counter, and Ag/AgCl as the references electrode. Moreover, the current working electrode was assessed utilizing a 3-electrode cell with 2 M KOH electrolytes. Galvanostatic charge–discharge (GCD), cyclic voltammetry (CV), and electrochemical impedance spectroscopies (EIS) are evaluated by an electrochemical workstation. The specific capacitances (C_{sp} , $F\ g^{-1}$) of the samples were calculated by Equation (1) based on CD plots [28–30]:

$$C_s = (I \times \Delta t) / m \times \Delta V \quad (1)$$

where Δt (s), I (A), m (g), and ΔV (V) designate the discharge times, currents, the mass of the electrode, and the applied potential, respectively.

3. Results and Discussion

3.1. Structure Characterization

The fabrication of the sulfur-deficient sheet-like $NiCo_2S_4$ nanoparticles on nickel foam is reported in Figure 1. The Ni foam consists of a porous nature composed of interconnected nickel skeletons, which possess the benefits of excellent electrical conductivities and richer porosity, consequently supplying numerous active sites for the redox process. Thus, the growth of sheet-like $NiCo_2S_4$ particles on the nickel skeleton was a reasonable possibility. First, the $NiCo_2S_4$ particles were acquired by a hydrothermal process accompanied by annealing at 400 °C for 1 h in the Ar atmosphere. The gained thin nanosheets were collected from nanosheets with a porous nature.

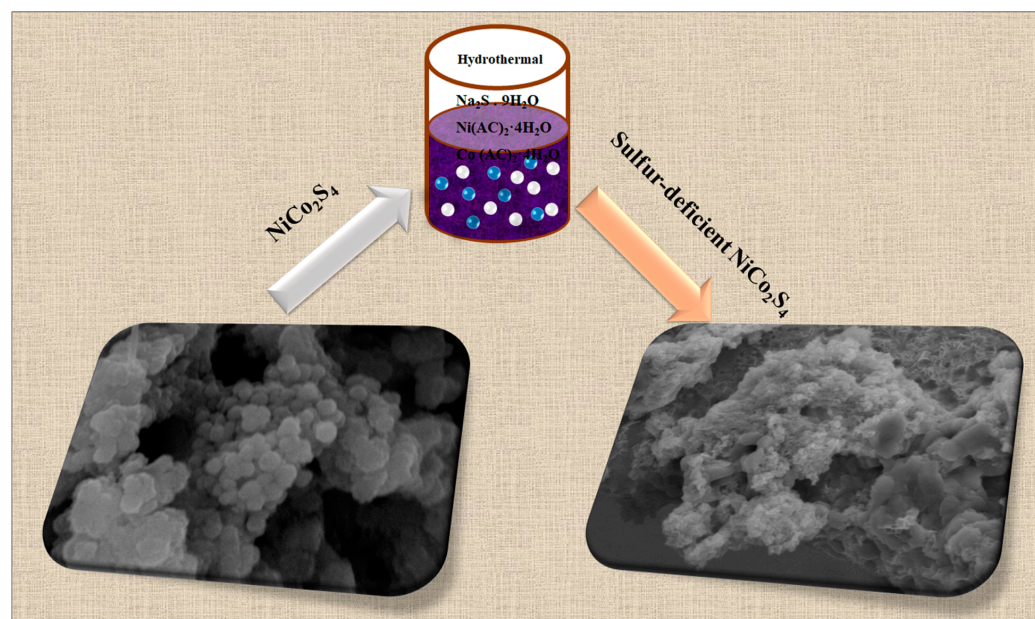


Figure 1. Schematic diagram illustrating the preparation of $NiCo_2S_4$ electrode and sulfur-deficient $NiCo_2S_4$ nanosheet composites on Ni foam substrate.

Figure 2 displays the microscopic morphology of the as-synthesized pure NiCo_2S_4 nanoparticles electrode and sulfur-deficient NiCo_2S_4 nanosheet composite samples. As illustrated in Figure 2a,b, the pure NiCo_2S_4 nanoparticles sample holds slightly incomplete developed and shapeless particle-type morphologies. Dissimilar to the pure NiCo_2S_4 nanoparticles, the sulfur-deficient NiCo_2S_4 nanosheets composite was made up of ultrathin-type nanosheets, self-assembling sheet-like particles with a median diameter of around $7\ \mu\text{m}$ (Figure 2c,d). This hierarchical nano-micro unique construction would supply abundant redox sites with higher active sites, condensing the diffusion networks of electrons/ions throughout the electrochemical reactions. In addition, the hydrothermal treatment affected the microstructure and crystallinity of the sulfur-deficient NiCo_2S_4 nanosheets composite, with the composite leading to the agglomeration of metallic nanoparticles and the electrochemical reactions of the electrode.

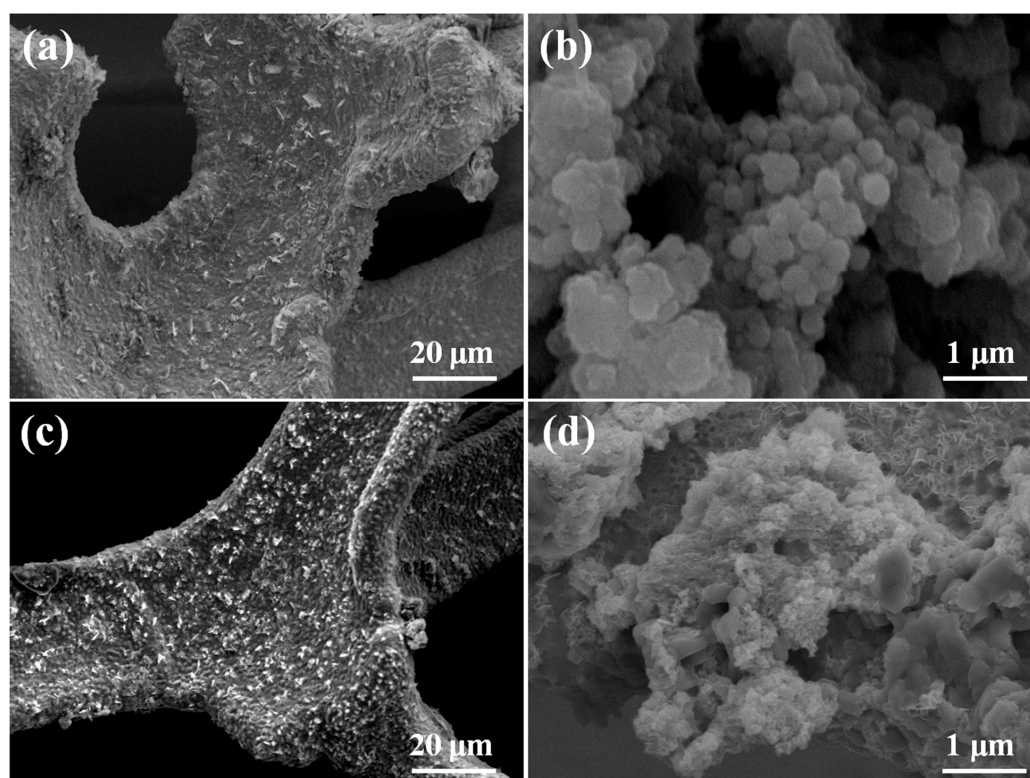


Figure 2. (a,b) SEM and FESEM images of pure NiCo_2S_4 nanoparticles electrode; and (c,d) SEM and FESEM images of the sulfur-deficient NiCo_2S_4 nanosheets composite.

Figure 3 displayed the TEM and HRTEM images of sulfur-deficient NiCo_2S_4 nanosheet composites. TEM images in Figure 3a further clarified that the metallic particles were flat and immobilized on the nickel foam skeleton porous structure. Figure 3b shows that, in the high-resolution TEM images, sulfur-deficient NiCo_2S_4 nanosheet composites possess lattice fringes, such that spaces of 0.24 and 0.28 nm were acquired; which are in excellent accordance with the (400) and (511) planes of NiCo_2S_4 , respectively [31,32]. On the other hand, the EDS elemental maps in Figure 3c–e depicted the uniform distributions of Ni, C, and S, revealing that the sulfur-deficient NiCo_2S_4 nanosheet composites are victoriously synthesized by a two-pot hydrothermal route.

The diffraction phase and purity of the as-reported pure NiCo_2S_4 nanoparticles electrode and sulfur-deficient NiCo_2S_4 nanosheet composites are investigated using X-ray diffraction analysis (Figure 4). The characteristic peaks at 26.7° , 31.5° , 38.4° , 47.5° , and 50.6° are attributed with the (220), (311), (400), (422), and (511) planes of the cubic NiCo_2S_4 phases, respectively (PDF#20-0782) [33,34]. It is obvious that all the good diffraction peaks of the NiCo_2S_4 would be ascribed to NiCo_2S_4 without clear diffractions correlated to the im-

purities, which evidences the successful preparation of sulfur-deficient NiCo_2S_4 nanosheet composites. Moreover, no additional peaks from the remaining crystallized planes could be gained from the electrode, noticing the excellent form of a pure NiCo_2S_4 sample.

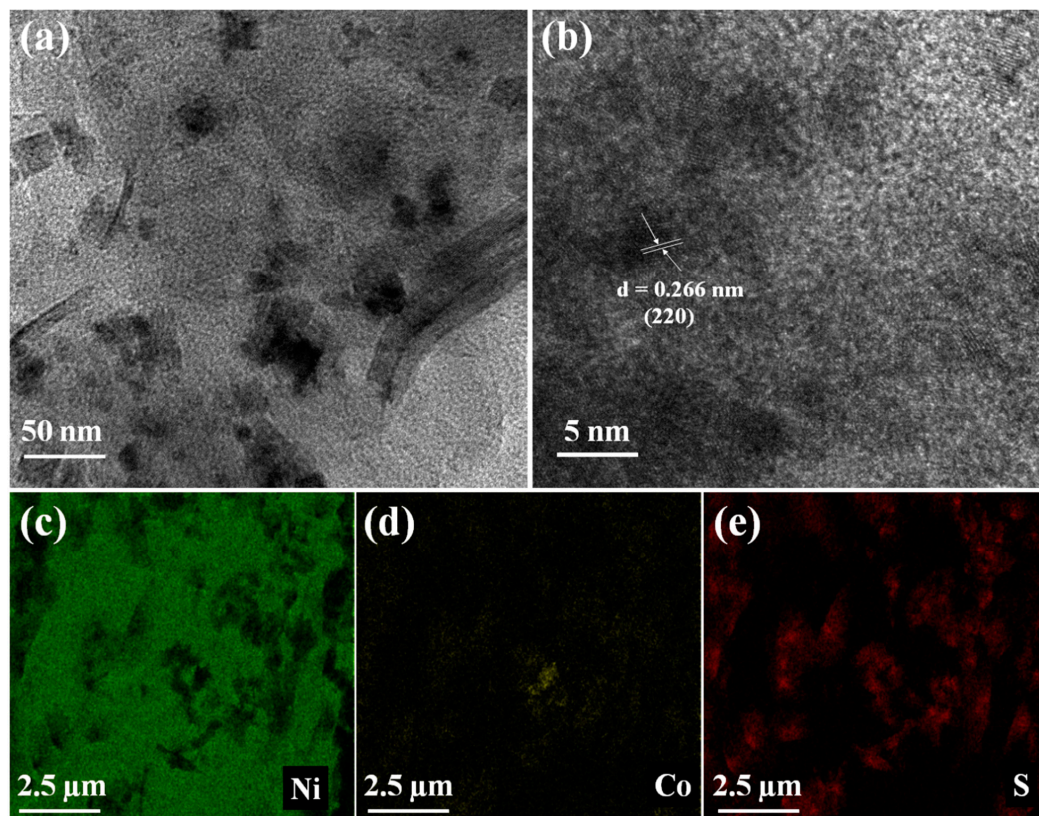


Figure 3. (a,b) TEM and HRTEM images, and (c–e) the elemental mapping images of sulfur-deficient NiCo_2S_4 nanosheets composite.

The chemical composition and elemental bonding states of the as-reported electrodes are fixed by using XPS spectra (Figure 4b–e). Figure 4b indicates a survey spectra of the sulfur-deficient NiCo_2S_4 nanosheets composites, which reports a dominance of Ni, C, and S [35]. The typical spectrum of Ni 2p (Figure 5b) and Co 2p (Figure 5c) corroborate the binary spin-orbits, respectively. In Figure 5b, in which there are the Ni 2p spectra, the 875.7 and 856.5 eV peaks are located from the Ni 2p_{1/2} and Ni 2p_{3/2}, respectively [36,37]. Accordingly, the Co 2p spectra in Figure 5c illustrate that the 802.4 and 783.3 peaks are located therein and associated with Co 2p [38–40]. Figure 5d displays the XPS spectrum of S 2p, revealing the existence of sulfide ions in the binary Ni-Co-S. The foremost peaks of S 2p were allocated at 168.9 eV. These noticed data were related to the earlier reporting [41]. The XPS findings recognize that the atomic ratios of Ni, Co, and S elements in the NiCo_2S_4 nanosheets were 1:2.93:4.94, which correlates with the findings output of the NiCo_2S_4 samples. The XRD and XPS results were fitting, considering the chemical elemental states and the formation compositions of the pure NiCo_2S_4 phases. Furthermore, the XPS spectra displayed the mixed chemical elemental states necessity of Ni 2p/Ni 3p and Co 2p/Co 3p, which play an important role in developing the entire electrochemical activities of the NiCo_2S_4 sample.

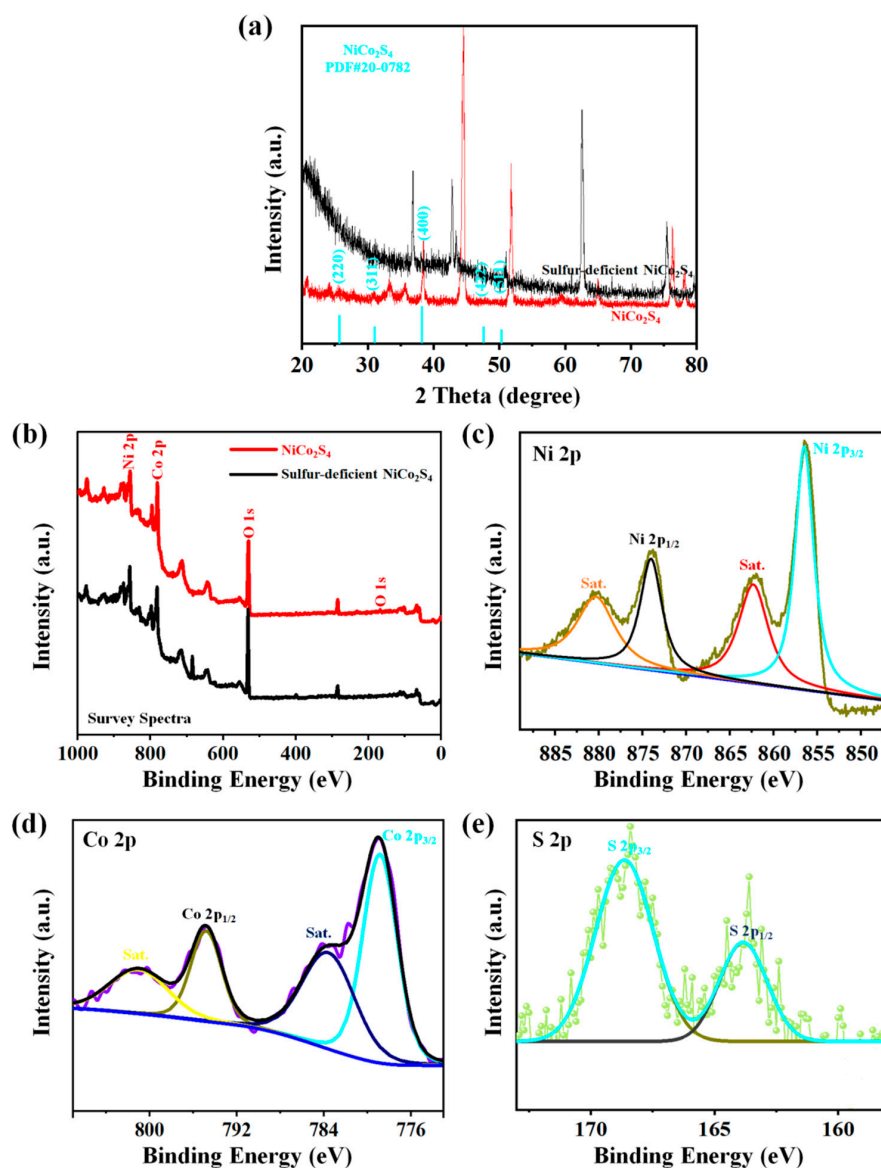


Figure 4. (a) XRD patterns of pure NiCo_2S_4 nanoparticles electrode and sulfur-deficient NiCo_2S_4 nanosheet composites. (b) XPS survey spectra, and (c–e) Ni 2p, Co 2p, and S 2p spectra for sulfur-deficient NiCo_2S_4 nanosheet composites.

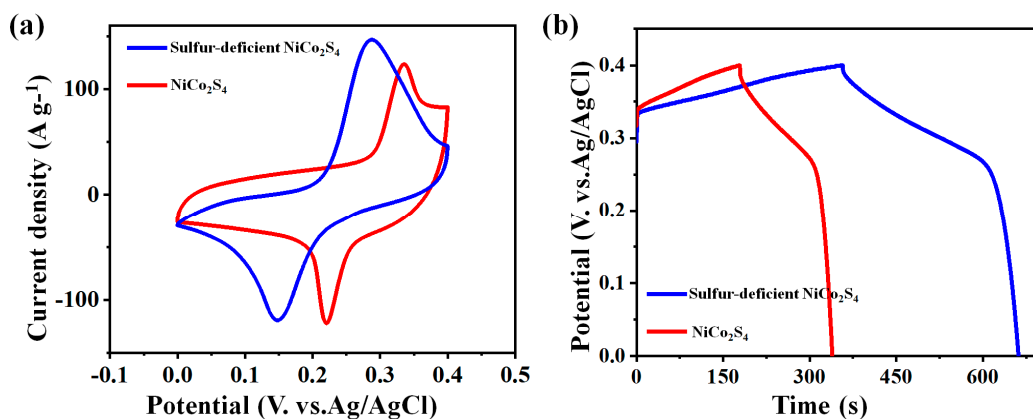
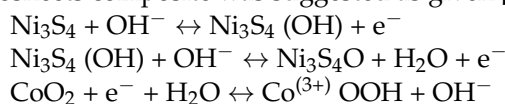


Figure 5. (a) CV curves and (b) GCD curves of pure NiCo_2S_4 nanoparticles electrode and sulfur-deficient NiCo_2S_4 nanosheet composites.

3.2. Electrochemical Performance

The CV and GCD plots were first organized to find out the electrochemical activities of the pure NiCo₂S₄ nanoparticles electrode and the sulfur-deficient NiCo₂S₄ nanosheet composites in the three-electrode setup. As illustrated in Figure 5a, a symmetric Faraday redox pairs plot was noticed from the CV plot, which is because of their highly reversible redox process amid Ni³⁺/Ni²⁺ and Co³⁺/Co²⁺ beneath alkaline solutions, resulting in the typical nature of PCs. The Faradaic possible reaction of the sulfur-deficient NiCo₂S₄ nanosheets composite was suggested as given [42,43]:



The CV plot region of the sulfur-deficient NiCo₂S₄ nanosheet composites was much larger than that of the pure NiCo₂S₄ nanoparticles electrode, revealing its high charging storing capability. Figure 5b illustrates the GCD plots of both electrodes, and clear charge/discharge platforms were denoted in all the particulars, further proposing its PCs properties. As expected, the sulfur-deficient NiCo₂S₄ nanosheet composites showed longer discharging times, which disclosed their higher capacitances.

Figure 6a discloses the CV plots of sulfur-deficient NiCo₂S₄ nanosheet composites at various sweep rates. Acquiescing with the polarizing effects of the sample electrodes, improving the sweep rates (5 to 100 mV s⁻¹) led to the cathode's peak shifting to fewer potentials, whereas the anode, peaking according to the reverse trends, moved to a higher potential. Figure 6b displays the GCD plot of the sulfur-deficient NiCo₂S₄ nanosheets composite electrode at different current values (2 to 20 A g⁻¹). The plot shapes are nearly similar and symmetrical, indicating its good electrochemical reversibility. Figure S1 demonstrates the CV and GCD plots of the pure NiCo₂S₄ nanoparticles electrode at various scan rates (5 to 100 mV s⁻¹) and current densities (2 to 20 A g⁻¹) in the 2M KOH aqueous electrolyte; this further exhibited its superior rate capabilities. According to the GCD results, the measured specific capacitance of both electrodes was reported in Figure 6c. At 1 A/g, the specific capacitances of the pure NiCo₂S₄ nanoparticles electrode and sulfur-deficient NiCo₂S₄ nanosheet composites were 564 and 971 F g⁻¹, respectively. These data values confirm that the hydrothermal route significantly overblows the specific capacitances of the composite. On the contrary, the higher sulfur-deficient NiCo₂S₄ nanosheets composite leads to the agglomeration of the metallic particle; thus, hindering the electrical migrations and holding back their electrochemical process. When the sulfur-deficient NiCo₂S₄ nanosheets composite is at 2 A g⁻¹, a specific surface region is large enough to reveal the required electrochemical active speeds to enhance the networks of the electrode sample and electrolytes.

In Figure 6d, the pure NiCo₂S₄ nanoparticles electrode and sulfur-deficient NiCo₂S₄ nanosheet composites reported smaller semi-circled diameters in the higher-frequencies area, and have roughly vertical lines in the lower frequencies region; this hinted that the sulfur-deficient NiCo₂S₄ nanosheet composites have optimal conductivities as well as quick charging transportation capabilities. The EIS curve is composed of the equivalent series resistance (R_s), the charge transfer resistance (R_{ct}), and Warburg diffusion resistance (R_w), which is related to the resistance of ionic diffusion in the electrolyte. The fitting results show that the R_{ct} values of the sulfur-deficient NiCo₂S₄ nanosheets composite and pure NiCo₂S₄ are 0.145 and 0.194 Ω, respectively. Therefore, it can be determined that the charge transfer resistance of the sulfur-deficient NiCo₂S₄ nanosheets composite is the smallest. Furthermore, the equivalent series resistance values of the sulfur-deficient NiCo₂S₄ nanosheets composite and pure NiCo₂S₄ are 1.732 and 0.831 Ω, respectively. The slope of the sulfur-deficient NiCo₂S₄ nanosheets composite is the largest, indicating that it has a high diffusivity of the electrolyte. In both cases, the R_s and R_{ct} values of the sulfur-deficient NiCo₂S₄ nanosheets composite has a strong dynamic response and electrical conductivity.

Figure 7 illustrates the long cycles of the sulfur-deficient NiCo_2S_4 nanosheet composites at 3 A g^{-1} . After 3500 long cycles of charges/discharges, the capacity retention of the sulfur-deficient NiCo_2S_4 nanosheet composites is still retained at 88.7%, further illustrating the outstanding life span of cycling stability analysis. From Table 1, the specified capacitance results data of the electrodes are demonstrated for comparison. Figure S2 illustrates the EIS curves of the sulfur-deficient NiCo_2S_4 before and after 3500 cycles of the stability test at 3 A g^{-1} .

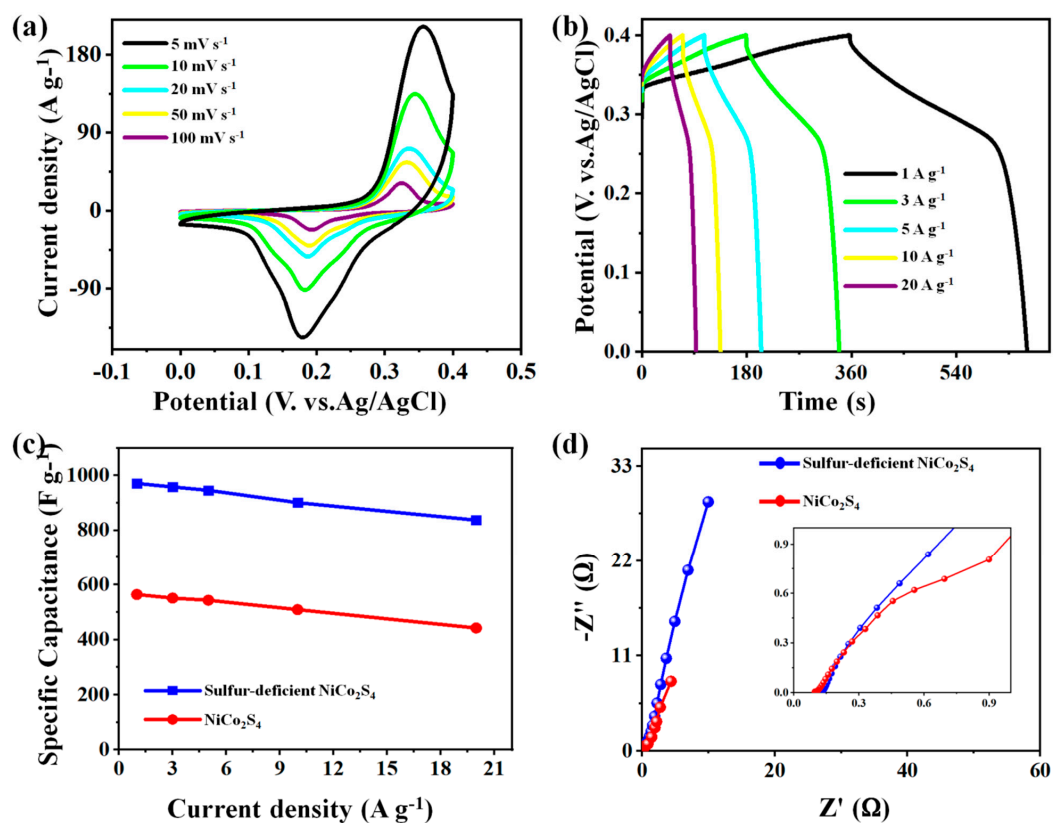


Figure 6. (a) CV curves and (b) GCD curves of the sulfur-deficient NiCo_2S_4 nanosheets composite electrode; (c) specific capacitances and (d) EIS curves of the pure NiCo_2S_4 nanoparticles electrode, and sulfur-deficient NiCo_2S_4 nanosheet composite electrodes.

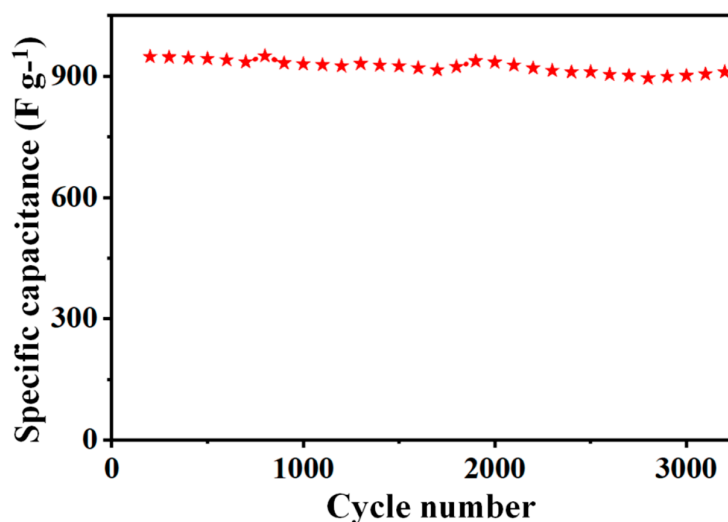


Figure 7. Cycling stability of the sulfur-deficient NiCo_2S_4 nanosheet composites over 3500 long cycles at a constant current density of 3 A g^{-1} .

Table 1. Comparison of the specific capacitance of the sulfur-deficient NiCo₂S₄ nanosheets composites electrode prepared in the present work and other reports in the literature.

Electrode	Preparation Method	Capacitance	Current Density	Ref.
NiCo ₂ S ₄ hollow hexagonal nanoplates	Sacrificial template method	437 F g ⁻¹	1 A g ⁻¹	[44]
NiCo ₂ S ₄ nanotube arrays	Hydrothermal method	738 F g ⁻¹	4 A g ⁻¹	[45]
NiCo ₂ S ₄ nanoflakes	Ionic layer adsorption	1076 F g ⁻¹	1 A g ⁻¹	[46]
NiCo ₂ S ₄ hollow nanoprisms	Sacrificial template method	895.2 F g ⁻¹	1 A g ⁻¹	[47]
NiCo ₂ S ₄ nanotube arrays	Electrodeposition	2.86 F cm ⁻²	4 mA cm ⁻²	[48]
NiCo ₂ S ₄ nanostructure	Precursor transformation method	1050 F g ⁻¹	2 A g ⁻¹	[49]
Sulfur-deficient NiCo ₂ S ₄ nanosheets	Hydrothermal method	971 F g ⁻¹	2 A g ⁻¹	This Work

4. Conclusions

We demonstrated a higher-efficiency approach to enhance the higher-performance electrode materials for supercapacitors by constructing rational nanomorphologies and increasing sulfur vacancies in NiCo₂S₄. The physical morphology data results exhibited that the hydrothermal route corresponds to the composite material crystallinity. By the data values, the as-developed sulfur-deficient NiCo₂S₄ nanosheet composites display a superior specific capacitance of 971 F g⁻¹ at 2 A g⁻¹ and capacitance retentions of 88.7% at 3 A g⁻¹ over 3500 long cycles. The excellent electrochemical capabilities would have corresponded to the involvement of sulfur vacancies and well-constructive superior specific area particle-like morphology that improves the electrode's conductivities, enhances activated sites for the electrochemical reactions, and encourages the electrolyte penetrations into the sample material. This study would open unique and favoring paths for the succession of future generations of high-performance materials for SCs. The developed electrode exhibited attractive potential in SCs applications.

Supplementary Materials: The following supporting information can be downloaded at: <https://www.mdpi.com/article/10.3390/molecules27217458/s1>, Figure S1: CV and GCD plots of pure NiCo₂S₄ nanoparticles electrode at various scan rates and current densities in aqueous electrolyte; Figure S2: EIS curves of the sulfur deficient NiCo₂S₄ before and after 3500 cycles of stability test at 3 A g⁻¹.

Author Contributions: Conceptualization, Y.A.K. and A.A.Y.; supervision and validation, M.M. and B.A.A.-A.; investigation and writing, Y.A.K., A.A.Y. and M.M.; investigation and visualization, B.A.A.-A. and S.-W.K.; validation, B.A.A.-A. All authors have read and agreed to the published version of the manuscript.

Funding: This research was funded by Researchers' supporting project number (RSP-2021/348), King Saud University, Riyadh, Saudi Arabia.

Institutional Review Board Statement: Not applicable.

Informed Consent Statement: Not applicable.

Data Availability Statement: No new data were created or analyzed in this study. Data sharing is not applicable to this article.

Acknowledgments: Researchers' supporting project number (RSP-2021/348), King Saud University, Riyadh, Saudi Arabia.

Conflicts of Interest: The authors declare no conflict of interest.

References

- Sharma, P.; Sundaram, M.M.; Watcharatharapong, T.; Jungthawan, S.; Ahuja, R. Tuning the Nanoparticle Interfacial Properties and Stability of the Core-Shell Structure in Zn-Doped NiMoO₄@AWO₄. *ACS Appl. Mater. Interfaces* **2021**, *13*, 56116–56130. [[CrossRef](#)] [[PubMed](#)]
- Sharma, R.; Sundaram, M.M.; Watcharatharapong, T.; Laird, D.; Euchner, H.; Ahuja, R. Zn Metal Atom Doping on the Surface Plane of One-Dimensional NiMoO₄ Nanorods with Improved Redox Chemistry. *ACS Appl. Mater. Interfaces* **2020**, *12*, 44815–44829. [[CrossRef](#)] [[PubMed](#)]

3. Yedluri, A.K.; Anitha, T.; Kim, H.-J. Fabrication of Hierarchical NiMoO₄/NiMoO₄ Nanoflowers on Highly Conductive Flexible Nickel Foam Substrate as a Capacitive Electrode Material for Supercapacitors with Enhanced Electrochemical Performance. *Energies* **2019**, *12*, 1143. [[CrossRef](#)]
4. Dahal, B.; Mukhiya, T.; Ojha, G.P.; Chhetri, K.; Tiwari, A.P.; Muthurasu, A.; Lee, M.; Chae, S.H.; Kim, T.; Chung, D.C.; et al. A multicore-shell architecture with a phase-selective ($\alpha + \delta$)MnO₂ shell for an aqueous-KOH-based supercapacitor with high operating potential. *Chem. Eng. J.* **2020**, *387*, 124028. [[CrossRef](#)]
5. Dahal, B.; Chhetri, K.; Muthurasu, A.; Mukhiya, T.; Tiwari, A.P.; Gautam, J.; Lee, J.Y.; Chung, D.C.; Kim, H.Y. Biaxial Stretchability in High-Performance, All-Solid-State Supercapacitor with a Double-Layer Anode and a Faradic Cathode Based on Graphitic-2200 Knitted Carbon Fiber. *Adv. Energy Mater.* **2021**, *11*, 2002961. [[CrossRef](#)]
6. Gautam, J.; Liu, Y.; Gu, J.; Ma, Z.; Dahal, B.; Chishty, A.N.; Ni, L.; Diao, G.; Wei, Y. Three-dimensional nano assembly of nickel cobalt sulphide/polyaniline@polyoxometalate/reduced graphene oxide hybrid with superior lithium storage and electrocatalytic properties for hydrogen evolution reaction. *J. Colloid Interface Sci.* **2022**, *614*, 642–654. [[CrossRef](#)]
7. Gautam, J.; Liu, Y.; Gu, J.; Ma, Z.; Zha, J.; Dahal, B.; Zhang, L.N.; Chishty, A.N.; Ni, L.; Diao, G.; et al. Fabrication of Polyoxometalate Anchored Zinc Cobalt Sulfide Nanowires as a Remarkable Bifunctional Electrocatalyst for Overall Water Splitting. *Adv. Funct. Mater.* **2021**, *31*, 2106147. [[CrossRef](#)]
8. Dahal, B.; Mukhiya, T.; Ojha, G.P.; Muthurasu, A.; Chae, S.H.; Kim, T.; Kang, D.; Kim, H.K. In-built fabrication of MOF assimilated B/N co-doped 3D porous carbon nanofiber network as a binder-free electrode for supercapacitors. *Electrochim. Acta* **2019**, *301*, 209–219. [[CrossRef](#)]
9. Kim, T.; Subedi, S.; Dahal, B.; Chhetri, K.; Mukhiya, T.; Muthurasu, A.; Gautam, J.; Lohani, P.C.; Acharya, D.; Pathak, I.; et al. Homogeneous Elongation of N-Doped CNTs over Nano-Fibrillated Hollow-Carbon-Nanofiber: Mass and Charge Balance in Asymmetric Supercapacitors Is No Longer Problematic. *Adv. Sci.* **2022**, *9*, 2200650. [[CrossRef](#)]
10. Yoon, J.H.; Kumar, Y.A.; Sambasivam, S.; Hira, S.A.; Krishna TN, V.; Zeb, K.; Uddin, W.; Kumar, K.D.; Obaidat, I.M.; Kim, S.; et al. Highly efficient copper-cobalt sulfide nano-reeds array with simplistic fabrication strategy for battery-type supercapacitors. *J. Energy Stor.* **2020**, *32*, 101988. [[CrossRef](#)]
11. Yedluri, A.K.; Kim, H.-J. Wearable super-high specific performance supercapacitors using a honeycomb with folded silk-like composite of NiCo₂O₄ nanoplates decorated with NiMoO₄ honeycombs on nickel foam. *Dalton Trans.* **2018**, *47*, 15545–15554. [[CrossRef](#)]
12. Kumar, Y.A.; Sambasivam, S.; Hira, S.A.; Zeb, K.; Uddin, W.; Krishna TN, V.; Kumar, K.D.; Obaidat, I.M.; Kim, H.J. Boosting the energy density of highly efficient flexible hybrid supercapacitors via selective integration of hierarchical nanostructured energy materials. *Electrochim. Acta* **2020**, *364*, 137318. [[CrossRef](#)]
13. Kulurumotlakatla, D.K.; Yedluri, A.K.; Kim, H.J. Hierarchical NiCo₂S₄ nanostructure as highly efficient electrode material for high-performance supercapacitor applications. *J. Energy Stor.* **2020**, *31*, 101619. [[CrossRef](#)]
14. Huang, Y.; Zhao, Y.; Bao, J.; Lian, J.; Cheng, M.; Li, H. Lawn-like FeCo₂S₄ hollow nanoneedle arrays on flexible carbon nanofiber film as binder-free electrodes for high-performance asymmetric pseudocapacitors. *J. Alloys Compd.* **2019**, *772*, 337–347. [[CrossRef](#)]
15. Elshahawy, A.M.; Li, X.; Zhang, H.; Hu, Y.T.; Ho, K.H.; Guan, C.; Wang, J. Controllable MnCo₂S₄ nanostructures for high performance hybrid supercapacitors. *J. Mater. Chem. A* **2017**, *5*, 7494–7506. [[CrossRef](#)]
16. Sun, W.; Du, Y.; Wu, G.; Gao, G.; Zhu, H.; Shen, J.; Zhang, K.; Cao, G. Constructing metallic zinc-cobalt sulfide hierarchical core-shell nanosheet arrays derived from 2D metal-organic-frameworks for flexible asymmetric supercapacitors with ultrahigh specific capacitance and performance. *J. Mater. Chem. A* **2019**, *7*, 7138–7150. [[CrossRef](#)]
17. Yang, Y.; Huang, W.; Li, S.; Ci, L.; Si, P. Surfactant-dependent flower- and grass-like Zn_{0.76}Co_{0.24}S/Co₃S₄ for high-performance all-solid-state asymmetric supercapacitors. *J. Mater. Chem. A* **2018**, *6*, 22830–22839. [[CrossRef](#)]
18. Li, H.; He, Y.; Dai, Y.; Ren, Y.; Gao, T.; Zhou, G. Bimetallic SnS₂/NiS₂@S-rGO nanocomposite with hierarchical flower-like architecture for superior high rate and ultra-stable half/full sodium-ion batteries. *Chem. Eng. J.* **2022**, *427*, 131784. [[CrossRef](#)]
19. Li, Y.; Qian, J.; Zhang, M.; Wang, S.; Wang, Z.; Li, M.; Bai, Y.; An, Q.; Xu, H.; Wu, F.; et al. Co-Construction of Sulfur Vacancies and Heterojunctions in Tungsten Disulfide to Induce Fast Electronic/Ionic Diffusion Kinetics for Sodium-Ion Batteries. *Adv. Mater.* **2020**, *32*, 2005802. [[CrossRef](#)]
20. Kumar, Y.A.; Kim, H.-J. Preparation and electrochemical performance of NiCo₂O₄@NiCo₂O₄ composite nanoplates for high performance supercapacitor applications. *New J. Chem.* **2018**, *42*, 19971–19978. [[CrossRef](#)]
21. Niu, L.; Wu, T.; Chen, M.; Yang, L.; Yang, J.; Wang, Z.; Kornyshev, A.A.; Jiang, H.; Bi, S.; Feng, G. Conductive Metal-Organic Frameworks for Supercapacitors. *Adv. Mater.* **2022**, e2200999. [[CrossRef](#)] [[PubMed](#)]
22. Lee, Y.S.; Kumar, Y.K.; Sambasivam, S.; Hira, S.A.; Zeb, K.; Uddin, W.; Reddy, S.P.R.; Kumar, K.D.; Obaidat, I.M.; Kim, H.J.; et al. CoCu₂O₄ nanoflowers architecture as an electrode material for battery type supercapacitor with improved electrochemical performance. *Nano-Struct. Nano-Objects* **2020**, *24*, 100618. [[CrossRef](#)]
23. Wan, H.; Jiang, J.; Yu, J.; Xu, K.; Miao, L.; Zhang, L.; Chen, H.; Ruan, Y. NiCo₂S₄ porous nanotubes synthesis via sacrificial templates: High-performance electrode materials of supercapacitors. *CrystEngComm* **2013**, *15*, 7649–7651. [[CrossRef](#)]
24. Chen, X.; Chen, D.; Guao, X.; Wang, R.; Zhang, H. Facile Growth of Caterpillar-like NiCo₂S₄ Nanocrystal Arrays on Nickel Foam for High-Performance Supercapacitors. *ACS Appl. Mater. Interfaces* **2017**, *9*, 18774–18781. [[CrossRef](#)] [[PubMed](#)]

25. Zhou, X.; Yue, X.; Dong, Y.; Zheng, Q.; Lin, D.; Du, X.; Qu, G. Enhancing electrochemical performance of electrode material via combining defect and heterojunction engineering for supercapacitors. *J. Colloid Interface Sci.* **2021**, *599*, 68–78. [[CrossRef](#)] [[PubMed](#)]
26. Huang, C.; Gao, A.; Yi, F.; Wang, Y.; Shu, D.; Liang, Y.; Zhu, Z.; Ling, J.; Hao, J. Metal organic framework derived hollow NiS@C with S-vacancies to boost high-performance supercapacitors. *Chem. Eng. J.* **2021**, *419*, 129643. [[CrossRef](#)]
27. Zhu, Y.; Wu, Z.; Jing, M.; Xuming, J.; Xuming, Y.; Song, W.; Ji, X. Mesoporous NiCo₂S₄ nanoparticles as high-performance electrode materials for supercapacitors. *J. Power Sources* **2015**, *273*, 584–590. [[CrossRef](#)]
28. Xie, P.; Yuan, W.; Liu, X.; Peng, Y.; Yin, Y.; Li, Y.; Wu, Z. Multifunctional surfactants for synthesizing high-performance energy storage materials. *Energy Storage Mater.* **2021**, *36*, 56–76. [[CrossRef](#)]
29. Lobato, B.; Suárez, L.; Guardia, L.; Centeno, T.A. Capacitance and surface of carbons in supercapacitors. *Carbon* **2017**, *122*, 434–445. [[CrossRef](#)]
30. Zhang, X.; Wang, Y.; Yu, X.; Tu, J.; Ruan, D.; Qiao, Z.J. High-performance discarded separator-based activated carbon for the application of supercapacitors. *Energy Storage* **2021**, *44*, 103378. [[CrossRef](#)]
31. Lin, L.; Liu, J.; Liu, T.; Hao, J.; Ji, K.; Sun, R.; Zeng, W.; Wang, Z. Growth-controlled NiCo₂S₄ nanosheet arrays with self-decorated nanoneedles for high-performance pseudocapacitors. *J. Mater. Chem. A* **2015**, *3*, 17652–17658. [[CrossRef](#)]
32. Yedluri, A.K.; Kulurumotlakatla, D.K.; Sangaraju, S.; Obaidat, I.M.; Kim, H.J. Facile synthesis of novel and highly efficient CoNi₂S₄-Ni(OH)₂ nanosheet arrays as pseudocapacitive-type electrode material for high-performance electrochemical supercapacitors. *J. Energy Stor.* **2020**, *31*, 101623. [[CrossRef](#)]
33. Wang, H.; Ren, Q.; Brett, D.J.L.; He, G.; Wang, R.; Key, J.; Ji, S. Double-shelled tremella-like NiO@Co₃O₄@MnO₂ as a high-performance cathode material for alkaline supercapacitors. *J. Power Sources* **2017**, *343*, 76–82. [[CrossRef](#)]
34. Zeng, Z.; Wang, D.; Zhu, J.; Xiao, F.; Li, Y.; Zhu, X. NiCo₂S₄ nanoparticles//activated balsam pear pulp for asymmetric hybrid capacitors. *CrystEngComm* **2016**, *18*, 2363–2374. [[CrossRef](#)]
35. Wang, C.; Wang, J.; Wu, W.; Qian, J.; Song, S.; Yue, Z.J. Feasibility of activated carbon derived from anaerobic digester residues for supercapacitors. *Power Sources* **2019**, *412*, 683–688. [[CrossRef](#)]
36. Brousse, T.; Bélanger, D.; Long, J.W. To Be or Not to Be Pseudocapacitive? *J. Electrochem. Soc.* **2015**, *162*, A5185. [[CrossRef](#)]
37. Gu, C.; Ge, X.; Wang, X.; Tu, J. Cation–anion double hydrolysis derived layered single metal hydroxide superstructures for boosted supercapacitive energy storage. *J. Mater. Chem. A* **2015**, *3*, 14228–14238. [[CrossRef](#)]
38. Chhetri, K.; Tiwari, A.P.; Dahal, B.; Ojha, G.P.; Mukhiya, T.; Lee, M.; Kim, T.; Chae, S.; Muthurasu, A.; Kim, H.Y. A ZIF-8-derived nanoporous carbon nanocomposite wrapped with Co₃O₄-polyaniline as an efficient electrode material for an asymmetric supercapacitor. *J. Electroanal. Chem.* **2020**, *856*, 113670. [[CrossRef](#)]
39. Chhetri, K.; Dahal, B.; Mukhiya, T.; Tiwari, A.P.; Muthurasu, A.; Kim, H.Y. Integrated hybrid of graphitic carbon-encapsulated Cu_xO on multilayered mesoporous carbon from copper MOFs and polyaniline for asymmetric supercapacitor and oxygen reduction reactions. *Carbon* **2021**, *179*, 89–99. [[CrossRef](#)]
40. Yang, Y.; Wang, X.; Huang, F.; Zhao, J.; Wang, X. Ni(OH)₂ nanodot-decorated Co–Co LDH/C hollow nanocages for a high performance supercapacitor. *Dalton Trans.* **2020**, *49*, 17310–17320. [[CrossRef](#)]
41. Zhang, J.; Wang, Z.; Deng, T.; Zhang, W. Ni(OH)₂ derived Ni-MOF supported on carbon nanowalls for supercapacitors. *NanoTechnology* **2021**, *32*, 195404. [[CrossRef](#)] [[PubMed](#)]
42. Cai, D.; Wang, D.; Wang, C.; Liu, B.; Wang, L.; Liu, Y.; Li, Q.; Wang, T. Construction of desirable NiCo₂S₄ nanotube arrays on nickel foam substrate for pseudocapacitors with enhanced performance. *Electrochim. Acta* **2015**, *151*, 35–41. [[CrossRef](#)]
43. Kumar, Y.A.; Kumar, K.D.; Kim, H.J. A novel electrode for supercapacitors: Efficient PVP-assisted synthesis of Ni₃S₂ nanostructures grown on Ni foam for energy storage. *Dalton Trans.* **2020**, *49*, 4050–4059. [[CrossRef](#)] [[PubMed](#)]
44. Pu, J.; Cui, F.; Chu, S.; Wang, T.; Sheng, E.; Wang, Z. Preparation and Electrochemical Characterization of Hollow Hexagonal NiCo₂S₄ Nanoplates as Pseudocapacitor Materials. *ACS Sustain. Chem. Eng.* **2014**, *2*, 809–815. [[CrossRef](#)]
45. Pu, J.; Wang, T.; Wang, H.; Tong, Y.; Lu, C.; Kong, W.; Wang, Z. Direct Growth of NiCo₂S₄ Nanotube Arrays on Nickel Foam as High-Performance Binder-Free Electrodes for Supercapacitors. *ChemPlusChem* **2014**, *79*, 577–583. [[CrossRef](#)]
46. Shinde, S.K.; Jalak, M.B.; Ghodake, G.S.; Maile, N.C.; Kumbhar, V.S.; Lee, D.S.; Fulari, V.J.; Kim, D.Y. Chemically synthesized nanoflakes-like NiCo₂S₄ electrodes for high-performance supercapacitor application. *Appl. Sur. Science.* **2019**, *466*, 822–829. [[CrossRef](#)]
47. Yu, L.; Zhang, L.; Wu, H.B.; Lou, X.W. Formation of Ni(x)Co(3-x)S₄ hollow nanoprisms with enhanced pseudocapacitive properties. *Angew. Chem. Int. Ed.* **2014**, *53*, 3711–3714. [[CrossRef](#)]
48. Xiao, J.; Wan, L.; Yang, S.; Xiao, F.; Wang, S. Design Hierarchical Electrodes with Highly Conductive NiCo₂S₄ Nanotube Arrays Grown on Carbon Fiber Paper for High-Performance Pseudocapacitors. *Nano Lett.* **2014**, *14*, 831–838. [[CrossRef](#)]
49. Chen, H.; Jiang, J.; Zhang, L.; Wan, H.; Qi, T.; Xia, D. Highly conductive NiCo₂S₄ urchin-like nanostructures for high-rate pseudocapacitors. *Nanoscale* **2013**, *5*, 8879–8883. [[CrossRef](#)]